Journal of Molecular Catalysis A: Chemical 313 (2009) 55–64

Contents lists available at ScienceDirect

Journal of Molecular Catalysis A: Chemical

journal homepage: www.elsevier.com/locate/molcata

Production of hydrogen by partial oxidation of methanol over bimetallic Au–Cu/TiO_2–Fe_2O_3 catalysts

Feg-Wen Chang*, Ti-Cheng Ou, L. Selva Roselin, Wun-Syong Chen, Szu-Chia Lai, Hsiao-Min Wu

Department of Chemical and Materials Engineering, National Central University, Chungli 32001, Taiwan

ARTICLE INFO

Article history:
Received 10 April 2009
Received in revised form 8 July 2009
Accepted 3 August 2009
Available online 8 August 2009

Keywords:
Au–Cu bimetallic catalyst
TiO_2–Fe_2O_3 binary support
Methanol partial oxidation
Hydrogen
Deposition–precipitation

ABSTRACT

Partial oxidation of methanol (POM) to produce H_2 was investigated over Au–Cu/TiO_2 and Au–Cu/TiO_2–Fe_2O_3 catalysts. The catalysts were prepared by deposition-precipitation method and characterized by XRD, TEM, HRTEM, ICP-AES, TPR, NH_3-TPD and XPS analyses. Detail study on the Au–Cu/TiO_2–Fe_2O_3 catalysts was performed to optimize Ti/Fe ratio, pH during preparation of the catalyst, calcination temperature and reaction temperature. The Au–Cu/TiO_2–Fe_2O_3 catalyst with Ti/Fe = 9/1 atomic ratio is more active and exhibits higher methanol conversion compared to the Au–Cu/TiO_2 catalyst. The higher activity of Fe-containing catalyst was attributed to the ability to supply reactive oxygen, thereby stabilize active gold species ($Au^{\delta+}$) in the catalyst. Studies on the optimization of pH during preparation of the Au–Cu/TiO_2–Fe_2O_3 catalyst and calcination temperature showed that the catalyst prepared at pH 7 and dried at 373 K (uncalcined) exhibited higher activity. The catalytic performance at various reaction temperatures shows that both methanol conversion and hydrogen selectivity are increased with increasing the temperature. A small increase in CO selectivity was observed beyond 523 K, which is due to the decomposition of methanol and reverse water gas shift at high temperatures.

1. Introduction

Fuel cells have recently attracted much attention as a potential device for energy transformation. Hydrogen is an excellent fuel for fuel cell application, because it is intrinsically clean and high thermal efficiencies [1]. Methanol has been recommended as the best source for hydrogen fuel among the high energy density liquid fuels, due to the high H/C ratio having a lower propensity for soot formation than other hydrocarbons, relatively low boiling point, easy storing and it reduce the risk of catalyst coking by the absence of C–C bonds [2]. Hydrogen can be obtained from methanol by several routes, such as steam reforming of methanol (SRM) [3,4], partial oxidation of methanol reaction (POM) [5–8], methanol decomposition (MD) [9,10] and oxidative steam reforming of methanol (OSRM) [11]. Partial oxidation of methanol is one of the suitable methods. The main advantage of POM is it exhibits an exothermic reaction with high reaction rates. In the literature, Cu- and Pd-based catalysts were commonly tested for POM [5–7,12,13]. The most important drawback of these catalysts is the formation of significant amount CO, which poisons the platinum electrode in the fuel cells. In recent years, supported gold nanoparticles have received much attention because of their unique catalytic properties for various oxidation and reduction reactions under mild conditions [14]. In our previous study we found that these catalysts are active for POM to produce hydrogen [15,16]. Catalytic properties of these gold nanoparticles depend on particle size, oxidation state of gold, the nature of the oxide support material and the interaction between gold nanoparticles and supports. Composite oxide supports have been successfully applied to stabilize small metal particles. Active supports can provide oxygen atoms and thus enhance activity; moreover, they are also capable of enhancing the stability of small gold particles. Addition of transition-metal oxides in supported gold catalysts increased the activity and stability of the catalysts for different reactions [17–21]. For example, the activity of Au/Al_2O_3 catalysts was improved by the addition of oxides of Ti, Cu, Ce, Fe and Li. In these metal oxide additives, copper showed higher activity and selectivity towards the desired product [17]. Furthermore, the increased activity of supported gold catalysts by the addition of Fe is reported in the literatures. The addition of Fe species in Au/MgO catalysts enhanced activity of the catalyst for CO oxidation, which was attributed to the ability to supply reactive oxygen [19]. Liu et al. [22] studied the Fe oxide-promoted Pt/γ-Al_2O_3 catalyst applied for the selective catalytic oxidation of CO in H_2. The Fe oxide is in intimate contact with the Pt to progress high CO activity. It interacts with Pt species and changes the electronic prosperities of the Pt particles. A dual site non-competitive mechanism for CO oxidation is created by providing oxygen from Fe oxide to the CO adsorbed on Pt. Golubina et al. [23] investigated the addi-

* Corresponding author. Tel.: +886 3 4227151x34202; fax: +886 3 4252296.
E-mail address: fwchang@cc.ncu.edu.tw (F.-W. Chang).

1381-1169/$ – see front matter © 2009 Elsevier B.V. All rights reserved.
doi:10.1016/j.molcata.2009.08.002

tion of Fe to Pd/C catalyst, which shows considerable increase of catalytic activity in hydrodechlorination (HDC) of hexachlorobenzene. In these catalysts, two different materials complement each other in surface stability, oxygen mobility and electronic properties to enhance the activity in the composite catalysts [18]. In addition, the existence of an oxygen reservoir on the support reduces the dependence of the activity on the metal particle size. Therefore the essential factor of controlling particle of Au is achieved by the addition of metal oxide additives. In our recent study, Au–Cu/TiO_2 catalyst was tested for POM to produce hydrogen and found that this catalyst was active for the formation of hydrogen [16]. As Fe addition can improve activity and stability of the catalyst, it is interesting to test the effect of addition of Fe in Au–Cu/TiO_2 catalyst.

In the present study, effect of addition of Fe species in Au–Cu/TiO_2 catalyst has been investigated for partial oxidation of methanol to produce hydrogen. The catalytic activity of Au–Cu/TiO_2–Fe_2O_3 catalyst was compared with Au–Cu/TiO_2 catalyst. The reaction parameters such as the pH during preparation of the catalyst, calcination temperature and reaction temperature on the activity of Au–Cu/TiO_2–Fe_2O_3 catalysts were optimized. To identify the surface morphology, composition, oxidation state and crystallite size, we employed several techniques such as transmission electron microscopy (TEM), high resolution transmission electron microscopy (HRTEM), inductively coupled plasma atomic emission spectroscopy (ICP-AES), X-ray diffraction (XRD), temperature-programmed reduction (TPR), NH_3 temperature-programmed desorption (NH_3-TPD) and X-ray photoelectron spectroscopy (XPS).

2. Experimental

2.1. Catalyst preparation

Preparation of Au–Cu/TiO_2–Fe_2O_3 catalyst involves two steps. In the first step, the binary support, TiO_2–Fe_2O_3 was prepared by impregnation method. The Ti:Fe molar ratio were chosen as 10:0, 9:1, 8:2 and 7:3. The required amount of $Fe(NO_3)_3{\cdot}9H_2O$ solution was added into TiO_2 powder (Degussa P-25), the slurry was stirred at 303 K for 2 h. The support slurry was dried in air at 373 K overnight and then calcined at 673 K for 4 h.

In the second step, Au–Cu/TiO_2–Fe_2O_3 (1 wt.% Au, 1 wt.% Cu) catalysts with a total metal loading of 2 wt.% were prepared by deposition–precipitation method [24], using tetrachloroauric acid ($HAuCl_4{\cdot}3H_2O$, 99.99%, Alfa Aesar), copper nitrate pentahemihydrate ($Cu(NO_3)_2{\cdot}2.5H_2O$, Riedel-deHaën) and TiO_2–Fe_2O_3 binary support. Typically, an aqueous solution of $HAuCl_4{\cdot}3H_2O$ and $Cu(NO_3)_2{\cdot}2.5H_2O$ were mixed with stirring at 343 K. The pH was adjusted to the desired value by 0.1N NaOH solution. This was followed by the addition of the TiO_2–Fe_2O_3 binary support. The slurry was then aged at 343 K for 2 h. The precipitates were filtered and washed carefully until all chlorine ions were removed. The precursors were dried at 373 K for 24 h and calcined at different temperatures for 4 h.

2.2. Catalyst characterization

The gold and copper content in the catalysts were measured by inductively coupled plasma atomic emission spectroscopy (Jobin Yvon JY-38S spectrometer). About 0.02 g of catalyst was dissolved by aqua regia (HNO_3:HCl in 1:3 ratio) and then microwaved for 15 min. The solution was cooled down and diluted within the detection limit of the instrument.

X-ray diffraction (XRD) measurement was performed using a Bruker D8A X-day diffractometer operated at 40 kV and 30 mA using Cu Kα radiation with a wavelength of 1.5406 Å. The scanning angle was from 10° to 80° at a rate of 0.05°/s.

Transmission electron microscopy (TEM) analysis was performed on a JEOL JEM-2000FX II, the operating voltage was at 160 kV. The preparation of specimen was described in detail elsewhere [20]. From each sample, the metal particles size was measured carefully in order to determine a justified average particle size and size distribution.

High resolution transmission electron microscopy (HRTEM) analysis was executed by Tecnai G2 HRTEM, the operating voltage was set at 200 kV. The lattice image and Fourier-transform pattern were acquired to identify the species and morphology in the catalysts.

The temperature-programmed reduction (TPR) experiment was performed by a U-shaped quartz micro-reactor, surrounded with a furnace controlled by a programmable controller. About 40 mg of the catalyst was pretreated under flowing Ar (50 ml/min) at 373 K for 45 min. The sample was cooled to room temperature after the pretreatment. A reducing gas composed of 5% H_2 and 95% Ar was employed at a flow rate of 50 ml/min, with a heating ramp of 10 K/min from 323 to 900 K. The consumption of hydrogen was determined by gas chromatography (GC) equipped with a thermal conductivity detector (TCD).

X-ray photoelectron spectroscopy (XPS) technique was employed to obtain the information of chemical states of Au and Cu in Au–Cu/TiO_2–Fe_2O_3 catalyst. The measurements were performed by a Thermo VG Scientific Sigma Probe spectrometer equipped the monochromatized Al Kα radiation (1486.6 eV). The binding energies were determined utilizing C 1s spectrum as reference at 285.0 eV.

The NH_3-TPD (ammonia TPD) was performed by a U-shaped quartz micro-reactor, surrounded with a furnace controlled by a programmable controller. About 100 mg of the catalyst was pretreated under flowing Ar (50 ml/min) at 373 K for 1 h. The sample was cooled to room temperature after the pretreatment. A pure NH_3 was induced at a flow rate of 30 ml/min and adsorbed at room temperature for 1 h. The purge gas Ar at a flow rate of 30 ml/min was used to remove the excess NH_3 for 1 h. Then rise the temperature with a heating ramp of 10 K/min from 323 to 1048 K. The desorbed NH_3 was determined by gas chromatography (GC) equipped with a thermal conductivity detector (TCD).

2.3. Catalytic activity measurements

Partial oxidation of methanol (POM) was performed using an apparatus, which has been described in detail elsewhere [24]. The reaction was carried out at 1 atm and at temperatures between 448 and 573 K, using a U-shaped quartz micro-reactor (i.d. = 4 mm). The micro-reactor was located in a programmable furnace with a type K thermocouple placed in the center of the catalyst bed. The carrier gas Ar and reactant O_2 were carried by two Brooks 5850E mass flow meters separately controlled by a mass flow controller (Protec Instrument Co. Ltd. Model: PC-540) to regulate the total flow rate at 60 ml/min. The molar ratio of O_2/CH_3OH was kept at 0.3 with a gas hourly space velocity (GHSV) of 48,000 h^{-1}. The products were analyzed by two on line gas chromatographs (GC) with thermal conductivity detector equipped with porapak Q and carbosieve S-II columns.

3. Results and discussion

3.1. Metal loading at various pH during preparation of the catalyst

Elemental analysis of the catalysts was performed to verify the Au, Cu contents in Au–Cu/TiO_2–Fe_2O_3 catalysts at various pH values during its preparation. The catalysts were prepared at different pH values in the range of 5–9 with a nominal Au and Cu loadings each of

Table 1
Surface properties of Au–Cu/TiO_2–Fe_2O_3 (1 wt.% Au, 1 wt.% Cu) catalysts.

Catalyst	Ti/Fe atomic ratio	pH	Calcination temperature (K)	Metal loading (wt.%)[a]		Average particle size of Au–Cu (nm)[b]
				Au	Cu	
Au–Cu/TiO_2–Fe_2O_3	9/1	5	Uncalcined	0.94	0.67	3.3
Au–Cu/TiO_2–Fe_2O_3	9/1	6	Uncalcined	0.83	0.85	3.2
Au–Cu/TiO_2–Fe_2O_3	9/1	7	Uncalcined	0.84	0.83	2.9
Au–Cu/TiO_2–Fe_2O_3	9/1	8	Uncalcined	0.60	0.94	2.7
Au–Cu/TiO_2–Fe_2O_3	9/1	9	Uncalcined	0.34	0.90	2.4
Au–Cu/TiO_2	10/0	7	Uncalcined	0.98	1.00	2.6
Au–Cu/TiO_2–Fe_2O_3	8/2	7	Uncalcined	0.88	0.86	3.4
Au–Cu/TiO_2–Fe_2O_3	7/3	7	Uncalcined	0.98	0.89	3.6
Au–Cu/TiO_2–Fe_2O_3	9/1	7	473	–	–	3.5
Au–Cu/TiO_2–Fe_2O_3	9/1	7	573	–	–	3.7
Au–Cu/TiO_2–Fe_2O_3	9/1	7	673	–	–	3.9
Au–Cu/TiO_2–Fe_2O_3[c]	9/1	7	Uncalcined	0.84	0.83	3.5

[a] ICP-AES method.
[b] Calculated from TEM data.
[c] After POM reaction at 523 K for 3 h.

1 wt.%. Table 1 shows the fraction of Au and Cu species incorporated at different pH during preparation of Au–Cu/TiO_2–Fe_2O_3 catalysts (Ti/Fe = 9/1). The amount of deposition of Au was decreased with rise in pH value and the decrease became more prominent at pH beyond 8. However, reverse behavior was observed in Cu deposition. The deposition of metals on the support is controlled by the composition of metal species in solution and charge of the support material at various pH values. The charge on the TiO_2–Fe_2O_3 support is pH dependent. The isoelectric point (IEP) value for TiO_2 and Fe_2O_3 is 6.2 and 8.5, respectively [25]. The compositions of the Au and Cu species in solution are pH dependent. The extent of hydrolysis of metal species increases with pH. The main species of Au in solution was transformed from $AuCl_4^-$ to $Au(OH)_nCl_{4-n}^-$ (n = 1–3) at pH > 6. The value of n was closed to 3 at pH > 6. Below the IEP value of the support, the surface was positive due to protonation of the surface hydroxyls; above IEP value of the support, the charge was negative due to removal of protons from the surface hydroxyls. This means that below the IEP value, electrostatic adsorption of the gold and copper anions were possible, as it was direct anion exchange [26]; the adsorption of the negatively charged $Au(OH)_nCl_{4-n}^-$ complex decreases rapidly above the IEP value. With increasing pH, the gold uptake from the solution decreased. At higher pH the surface was negatively charged resulting in an electrostatic repulsion of gold containing anions; this probably accounts for the fall in the gold contents higher than pH 8. These results are in agreement with previous literature [27–29]. The reverse behavior of copper may be due to the formation of precipitate of Cu compound, malachite $Cu_2(CO_3)(OH)_2$, which was significantly formed as a contaminant at pH 7 compared with pH 5 [29].

3.2. XRD

Fig. 1 shows the X-ray diffraction patterns of Au–Cu/TiO_2 and Au–Cu/TiO_2–Fe_2O_3 with different Ti/Fe ratio dried at 373 K. In all the catalyst samples, titania shows peaks that corresponds to a mixture of anatase and rutile phase with the anatase phase dominating over the rutile phase. The crystallinity of TiO_2 was lowered with raising Fe contents in the support. In Au–Cu/TiO_2–Fe_2O_3, Fe is existed as Fe_2O_3 and Fe_3O_4. Diffraction peaks which contributed from Fe_2O_3 were found at 2θ = 33.2°, 35.6°, 49.5° and 66.8°. With increasing Fe content in the binary support, the intensity of these peaks became stronger. In addition to Fe_2O_3, a small peak for Fe_3O_4 was observed at 2θ = 36.8° (JCPDS 26-1136). The different phases of Fe oxide combined with TiO_2 contain more defects on the surface of the support; this should also strengthen metal-support interactions, and therefore, prevent metal agglomerating into larger particles. In all the samples, small intense diffraction peaks for

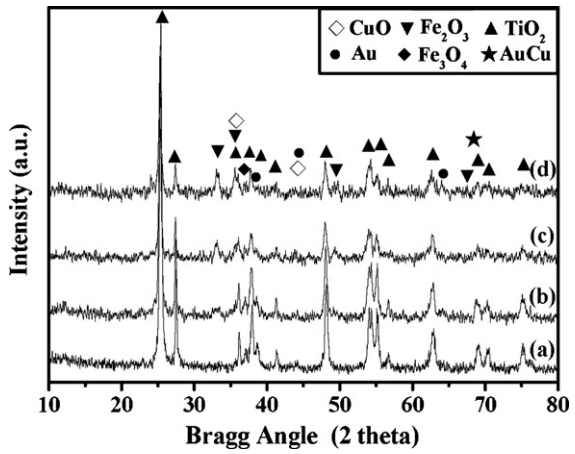

Fig. 1. XRD patterns of: (a) Au–Cu/TiO_2 (1–1 wt.%); (b) Au–Cu/TiO_2–Fe_2O_3 (1–1 wt.%, Ti/Fe = 9/1); (c) Au–Cu/TiO_2–Fe_2O_3 (1–1 wt.%, Ti/Fe = 8/2); (d) Au–Cu/TiO_2–Fe_2O_3 (1–1 wt.%, Ti/Fe = 7/3) (uncalcined, dried at 373 K; pH 7).

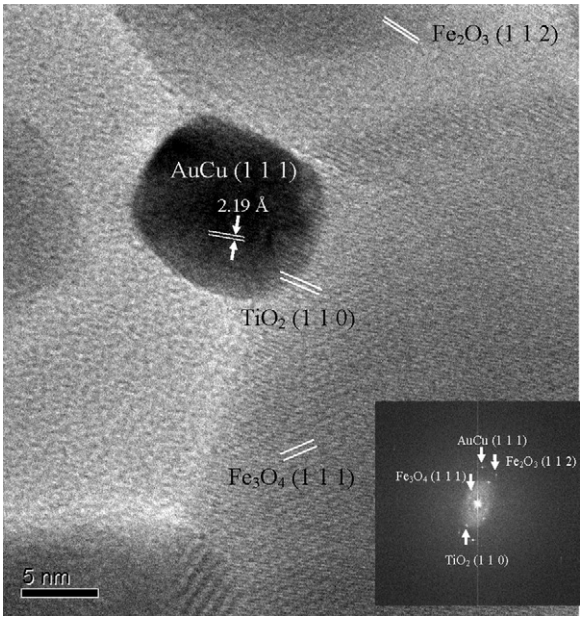

Fig. 2. HRTEM and Fourier transform images of Au–Cu/TiO_2–Fe_2O_3 (1–1 wt.%, Ti/Fe = 9/1) catalyst (uncalcined, dried at 373 K; pH 7).

metallic Au at $2\theta = 38.2^\circ$ and 44.4° were detected. The low intensity of these peaks may be due to the presence of small gold particles which are highly dispersed on the support. As the diffraction peak at $2\theta = 49.8^\circ$ for Au_2O_3 (JCPDS 24-0462) is merged with Fe_2O_3 diffraction peak at 49.4°, the presence of Au_2O_3 could not be confirmed by XRD analysis. The peaks correspond to CuO was observed at $2\theta = 35.4^\circ$ and 44.2°. However, the peak at 44.2° is superimposing with the Au^0 peak at 44.4°. Other copper species such as Cu_2O and metallic Cu were not detected by XRD analysis. XPS analysis was subsequently adapted to identify the chemical state of Au and Cu species and was reported in Section 3.5.

3.3. TEM and HRTEM

The detail morphology of the Au–Cu/TiO_2–Fe_2O_3 catalyst was examined by high resolution transmission electron microscopy (HRTEM). The Fourier transform technique was also employed to confirm the metal oxide species in the catalyst. The Au–Cu particle was detected by the lattice space from the lattice fringe and Fourier transform images in Fig. 2. The lattice space of Au–Cu (1 1 1) particles is 2.19 Å, which is consistent with the results reported by Llorca et al. [30]. The higher electron affinity of Au is compared with that of Cu led to an electron transfer from the Cu to Au. This interaction of Au and Cu may increase in catalytic activity for the Au–Cu/TiO_2–Fe_2O_3 catalysts. Other species, such as Fe_2O_3 (1 1 2) (2.36 Å, JCPDS 47-1409), Fe_3O_4 (1 1 1) (4.67 Å, JCPDS 26-1136) and TiO_2 (1 1 0) (3.25 Å, JCPDS 34-0180) were also observed in Fig. 2. The XRD analysis failed to identify the Au–Cu crystalline due to the overlap of Au–Cu ($2\theta = 48.2^\circ$) with the TiO_2 diffraction peak at $2\theta = 48.1^\circ$. The lattice fringe of the TiO_2–Fe_2O_3 binary support is also observed in the image. The Au–Cu particle and the support thus appeared in tight contact exhibiting specific crystal orientation. In addition to Fe_2O_3, Fe_3O_4 also exists in the binary support. It is well understood that the Fe_3O_4 exists in the support even after calcination at 673 K for 4 h during the binary support preparation. The HRTEM image shows that the Au–Cu particles are embedded on the binary support.

The particle size of Au–Cu in bimetallic Au–Cu/TiO_2–Fe_2O_3 catalysts with different Ti/Fe ratio was analyzed by TEM technique. Fig. 3 demonstrates that Au–Cu particles were deposited on the support homogeneously. Detail data of average particle size of Au–Cu are summarized in Table 1. The average size of Au–Cu particle increased slightly with increasing Fe contents in the Au–Cu/TiO_2–Fe_2O_3 catalysts. The average particle size of Au–Cu is 2.9, 3.4 and 3.6 nm corresponding to the Ti/Fe composition at 9/1, 8/2 and 7/3, respectively. Increase in particle size of metal by the

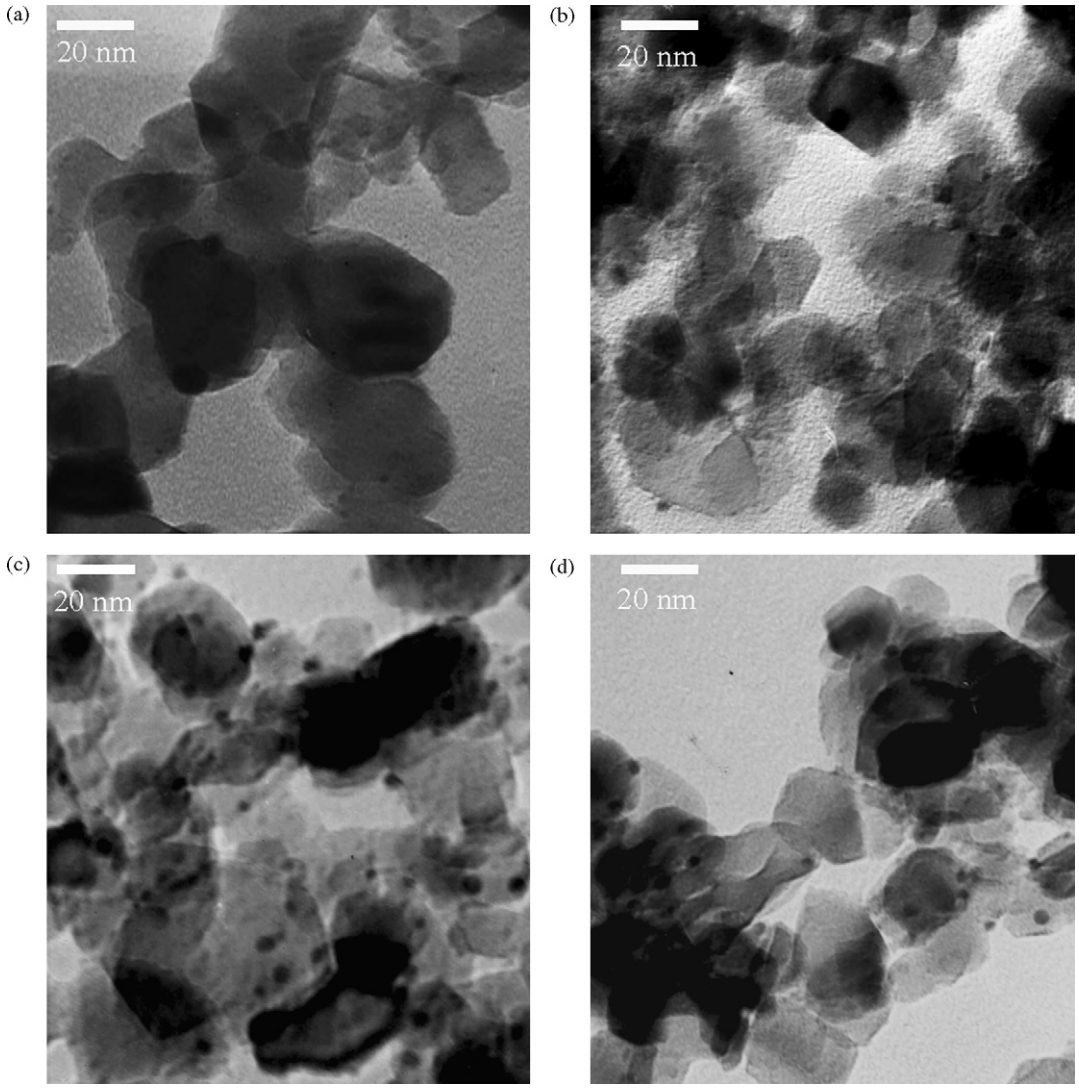

Fig. 3. TEM images of: (a) Au–Cu/TiO_2 (1–1 wt.%); (b) Au–Cu/TiO_2–Fe_2O_3 (1–1 wt.%, Ti/Fe = 9/1); (c) Au–Cu/TiO_2–Fe_2O_3 (1–1 wt.%, Ti/Fe = 8/2); (d) Au–Cu/TiO_2–Fe_2O_3 (1–1 wt.%, Ti/Fe = 7/3) catalyst (uncalcined, dried at 373 K; pH 7).

addition of metal oxide additives is also evidenced in the literature. For example, Chang et al. [31] reported that the addition of MnO_2 in Au/TiO_2 slightly enlarged the particle size of Au. Schubert et al. [19] found that in Au/Fe_2O_3-MgO catalyst with increasing Fe content, the average particle diameter of Au was increased. It also agrees with our previous work on Au/TiO_2–Fe_2O_3 catalyst [20]. The influence of calcination temperature on the particle size of Au–Cu in Au–Cu/TiO_2–Fe_2O_3 catalysts was also studied in detail. The results were summarized in Table 1. In uncalcined sample, average particle size of Au–Cu is 2.9 nm. Major fraction of Au–Cu particles is in the range of 1.3–5 nm, very few particles have the diameter between 5 and 10 nm. After calcination at 473 K, the mean particle size of Au–Cu became slightly larger than the uncalcined sample. In this sample, major fraction of Au–Cu particles is in the range of 1.3–5.3 nm and exhibited an average particle size of 3.5 nm. Previous studies on supported Au catalysts also showed similar larger Au particles with increasing calcination temperature [32,33]. Rising calcination temperature to 573 K, major fraction of Au–Cu particles is in the range of 1.5–5.5 nm with an average value of 3.7 nm. After calcination at 673 K, most particles varied between 2.7 and 7.3 nm, the average particle size is estimated as 3.9 nm. It is important to note that the mean size of Au–Cu particles is not affected much even after calcination at 673 K. In our previous study we observed that the particle size of Au in Au/TiO_2 sample was increased from 2.9 to 4.3 nm after calcination at 673 K [24]. Hua et al. [34] reported that increasing calcination temperature from 573 to 623 K, the mean diameter of Au particles in Au/Fe_2O_3 was increased from 5.8 to 7.7 nm. In the present study, the presence of binary support in Au–Cu/TiO_2–Fe_2O_3 catalyst preserved the Au metal particles during calcination process to a large extent. To understand the stability of the catalyst during reaction, the particle size of Au–Cu in the catalyst after catalytic test was determined. It is noteworthy that there was only a slight increase in metal particles after catalytic test at 523 K for 3 h. The metal particle size was increased from 2.9 to 3.5 nm. In our previous study the Au particle size in Au/TiO_2 catalyst was increased from 2.9 to 7.4 nm after the catalytic test at 523 K for 2 h [24]. This result confirmed that the presence of binary support in Au–Cu/TiO_2–Fe_2O_3 catalysts preserved the metal particle size during POM reaction. Therefore, the essential factor of small metal particle in supported catalysts has been fulfilled by the presence of binary support in the catalyst sample.

3.4. TPR

TPR profiles of Au–Cu/TiO_2 catalyst and Au–Cu/TiO_2–Fe_2O_3 catalyst at different Ti/Fe ratio are shown in Fig. 4. The Au–Cu/TiO_2 sample (Fig. 4a) showed a reduction peak at 349 K with a small shoulder at 371 K. The peak at 349 K is attributed to the reduction of CuO and oxidic Au to Cu_2O and metallic Au, respectively. Reduction of both species is coexisted at this temperature. The shoulder peak at 371 K was due to the reduction of Cu_2O to metallic copper. When Fe is introduced in Au–Cu/TiO_2, the reduction peaks for Au and Cu oxides shifted to higher temperature (Fig. 4b–d). In addition, the intensity of low temperature reduction peak is increased. The increased reduction temperature indicated that the addition of iron led to an increase in the interaction between gold, copper and TiO_2 species. The reduction peak of Au and Cu content was combined with the reduction of Fe species associated with them. With the increase of Fe amount, more Fe species reduced at low temperature which overlaps with Au and Cu. The reduction peaks for Fe_2O_3 in Au–Cu/TiO_2–Fe_2O_3 catalysts are consisted of one low temperature peak between 502 and 547 K and a broad peak between 686 and 832 K. The low temperature peak corresponds to the reduction of Fe_2O_3 to Fe_3O_4. The broad features of the reduction peak between 686 and 832 K correspond to two stage subsequent reduction of Fe_3O_4 to FeO and FeO to Fe. Nevertheless the two stage reduction

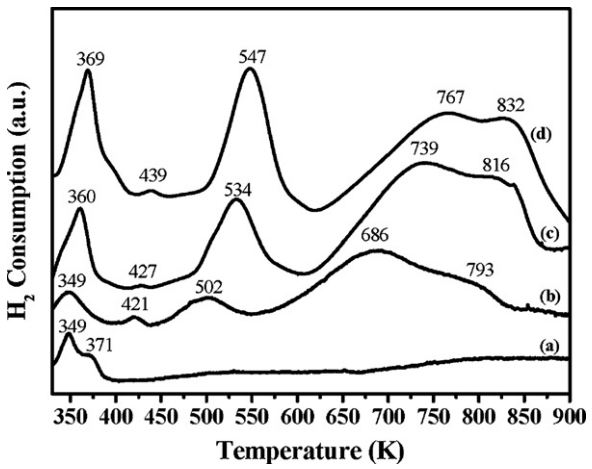

Fig. 4. TPR profiles of: (a) Au–Cu/TiO_2 (1–1 wt.%); (b) Au–Cu/TiO_2–Fe_2O_3 (1–1 wt.%, Ti/Fe = 9/1); (c) Au–Cu/TiO_2–Fe_2O_3 (1–1 wt.%, Ti/Fe = 8/2); (d) Au–Cu/TiO_2–Fe_2O_3 (1–1 wt.%, Ti/Fe = 7/3) (uncalcined, dried at 373 K; pH 7).

peaks can be clearly seen at higher amount of Fe. The specific reduction peaks for Fe_2O_3 to Fe_3O_4 and Fe_3O_4 to FeO shifted towards lower temperature for all Au–Cu/TiO_2–Fe_2O_3 catalysts compared to bulk Fe_2O_3. The enhanced reducibility of Fe_2O_3 is due to the effect of the hydrogen spillover from the metallic phase to the support [35]. On the other hand, at higher addition of Fe species, these peaks were shifted to higher temperature. This is due to excess Fe may not involve in interaction with Au and Cu species. The amount of H_2 consumed was dependent on the Fe contents in reduction region of the iron oxide. It is reasonable that more Fe in the catalysts consume more H_2 during TPR process as seen in Fig. 4b–d.

The TPR profile of Au–Cu/TiO_2–Fe_2O_3 catalyst calcined at different temperatures are presented in Fig. 5. The samples showed three reduction peaks along with a broad peak at high temperature. These peaks are assigned to the reduction of Au, Cu and Fe oxides to its corresponding metallic species. The uncalcined sample (Fig. 5a) shows a reduction peak centered at 349 K, which corresponds to the combination of reduction of Au_xO_y to Au^0 and highly dispersed small CuO particles to Cu_2O. The peak located at 421 K revealed the reduction of Cu_2O to Cu^0. With increasing calcination temperature, both peaks shifted to higher temperature. The higher reduction temperature indicates the increased crystallite size of CuO with increasing calcination temperature. It was reported that larger CuO crystallites reduced at high temperature [36]. The reduction peaks at 502 and 686 K are ascribed to the reduction of Fe_2O_3

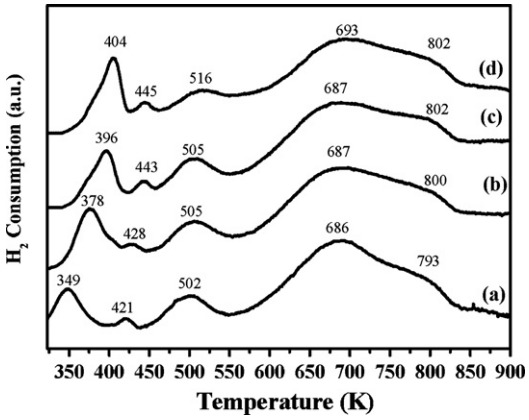

Fig. 5. TPR profiles of Au–Cu/TiO_2–Fe_2O_3 (1–1 wt.%, Ti/Fe = 9/1) catalysts calcined at different temperatures: (a) uncalcined; (b) calcined at 473 K; (c) calcined at 573 K; (d) calcined at 673 K (pH 7).

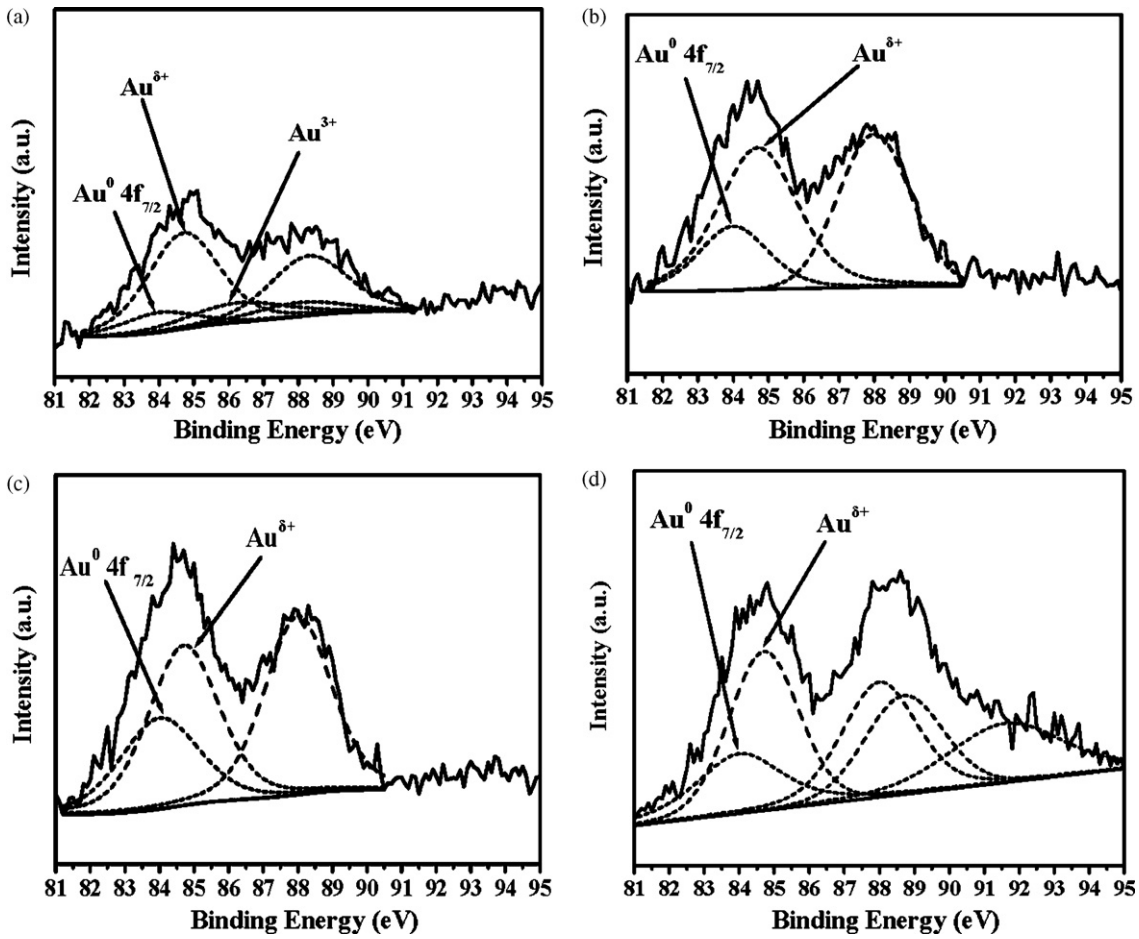

Fig. 6. XPS spectra of Au 4f region for Au–Cu/TiO_2–Fe_2O_3 (1–1 wt.%, Ti/Fe = 9/1) catalysts calcined at different temperatures: (a) uncalcined; (b) calcined at 473 K; (c) calcined at 573 K; (d) after POM reaction at 523 K for 3 h.

to Fe_3O_4 and Fe_3O_4 to FeO, respectively. There is no obvious difference of the reduction temperature for these species with increasing calcination temperature.

3.5. XPS

X-ray photoelectron spectroscopy (XPS) technique was employed to get information on the chemical states of Au, Cu species in Au–Cu/TiO_2–Fe_2O_3 catalysts at different calcination temperatures and after POM reaction. XPS spectra of Au 4f level for Au–Cu/TiO_2–Fe_2O_3 catalysts calcined at different temperatures and after POM reaction at 523 K are presented in Fig. 6. Each Au species shows two peaks correspond to the Au $4f_{7/2}$ and the Au $4f_{5/2}$ transitions. The XPS spectra of Au $4f_{7/2}$ level were deconvoluted with binding energy of 84, 84.7 and 86.2 eV for Au^0, $Au^{\delta+}$ and Au^{3+}, respectively [37,38]. The corresponding surface distributions of Au and Cu species in the Au–Cu/TiO_2–Fe_2O_3 catalysts are presented in Table 2. There existed Au^0 (14.1%), $Au^{\delta+}$ (67.1%) and Au^{3+} (18.8%) species in the uncalcined Au–Cu/TiO_2–Fe_2O_3 sample (Fig. 6a and Table 2). After calcination the intensity of the peaks shifted to lower binding energy. This shows that the composition of different gold species was changed in the sample. Small fractions of cationic Au species are converted to metallic Au species after calcination process. Nevertheless, complete reduction of cationic gold species to metallic gold was not observed by the existence of $Au^{\delta+}$ (47.4%) species after calcination at 673 K for 4 h (Fig. 6c). In the previous study it was reported that in Au/Fe_2O_3 catalyst the cationic gold was completely reduced to metallic gold after calcination at 673 K [34]. This suggests that the existence of reducible copper and iron species in Au–Cu/TiO_2–Fe_2O_3 catalysts stabilized the cationic gold species even after calcination at 673 K. Fig. 6d shows the Au 4f region of the uncalcined Au–Cu/TiO_2–Fe_2O_3 catalyst after POM reaction. About 21.4% of the oxidized Au species were reduced to metallic Au (Table 2). It is important to note that the Au species was not reduced to metallic form completely. Fig. 7 shows the X-ray photoelectron spectra of Cu $2p_{3/2}$ core level for Au–Cu/TiO_2–Fe_2O_3 catalysts calcined at different temperatures and after exposure to POM reaction at 523 K. The Cu $2p_{3/2}$ regions

Table 2
XPS data of Au $4f_{7/2}$ and Cu $2p_{3/2}$ region for different Au–Cu/TiO_2–Fe_2O_3 catalysts.

Sample	Au^0 (%)	$Au^{\delta+}$ (%)	Au^{3+} (%)	Cu^0 (%)	Cu_2O (%)	CuO (%)	$Cu(OH)_2$ (%)
Au–Cu/TiO_2–Fe_2O_3 uncalcined	14.1	67.1	18.8	0	76.1	22.0	1.9
Au–Cu/TiO_2 -Fe_2O_3 calcined at 473 K	25.1	74.9	0	0	39.7	60.3	0
Au–Cu/TiO_2 -Fe_2O_3 calcined at 573 K	38.7	61.3	0	0	39.1	60.9	0
Au–Cu/TiO_2 -Fe_2O_3 calcined at 673 K	52.6	47.4	0	0	32.8	67.2	0
Au–Cu/TiO_2–Fe_2O_3 uncalcined, after POM reaction	35.5	64.5	0	0	52.9	47.1	0

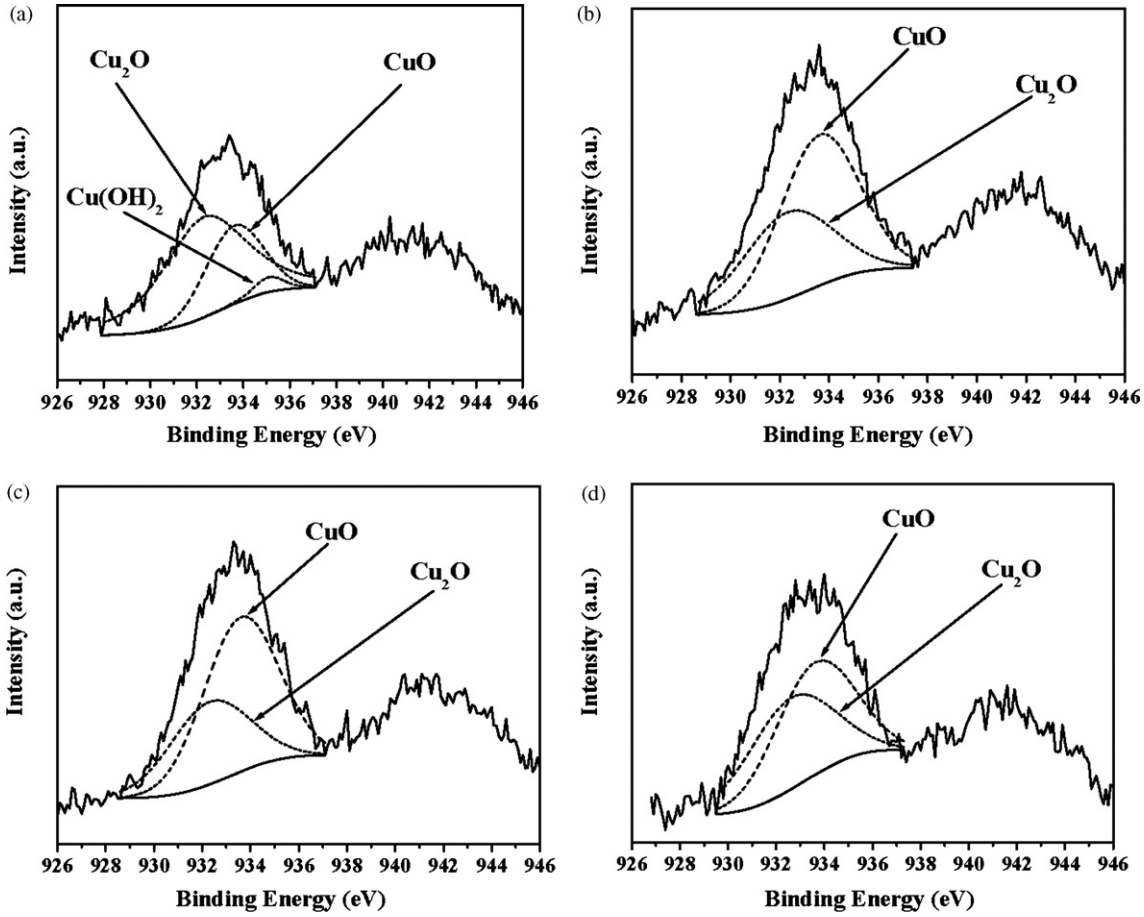

Fig. 7. XPS spectra of Cu 2p region for Au–Cu/TiO_2–Fe_2O_3 (1–1 wt.%, Ti/Fe = 9/1) catalysts calcined at different temperatures: (a) uncalcined; (b) calcined at 473 K; (c) calcined at 573 K; (d) after POM reaction at 523 K for 3 h.

were deconvoluted into different copper species in the catalysts. The peaks at 932.3, 934 and 934.8 eV were contributed by Cu_2O, CuO and $Cu(OH)_2$, respectively [37,39,40]. The compositions of different copper species in Au–Cu/TiO_2–Fe_2O_3 catalysts calcined at different temperatures and after exposure to POM reaction at 523 K were listed in Table 2. In the uncalcined sample and the sample after calcination, copper is existed as CuO and Cu_2O species. The quantity of Cu_2O species was increased after exposure to POM reaction at 523 K (Fig. 7d). This might be resulted through part of CuO reduced to Cu_2O by H_2 produced by POM reaction. Therefore, the Cu_2O and CuO species were coexisted in the catalyst after POM reaction. This is confirmed by Cu LMM XPS peaks observed at 916.6 eV (Cu_2O) [41].

3.6. NH_3-TPD

The NH_3-TPD technique was employed to determine the acidic sites in the Au–Cu/TiO_2–Fe_2O_3 catalysts with various Ti/Fe ratios in support. The results of NH_3-TPD analysis of the catalysts were performed in the temperature range of 323–1048 K are shown in Fig. 8. As defined in the literature, the amount of NH_3 desorbed below 473 K is a measure of weak acidic sites; 473–623 K range corresponds to intermediate acidic sites, and above 623 K represents strong acidic sites [42]. It showed two distinctive desorption regions where as the high temperature peak represents the NH_3 desorbed from the stronger acidic sites and the medium-low temperature peak represents the NH_3 desorbed from the intermediate and weak acidic sites. The quantities of NH_3 desorption are given in Table 3 which is stated that the addition of Fe species into the support increases the strong acidic sites. On the other hand, the total acidic sites decreased with the increasing amount of Fe. Also, the temperatures of the strongly adsorbed state for different samples were different. The high-temperature is peak presented at higher temperature on the Au–Cu/TiO_2 catalyst, indicating a higher desorption activation energy [43]. The desorption of strong acidic sites from 946 K shifts to relative low temperature at 871 K for the Ti/Fe = 9/1 sample compared to the Ti/Fe = 10/0 sample. By increasing more Fe species, the temperature of the strong desorp-

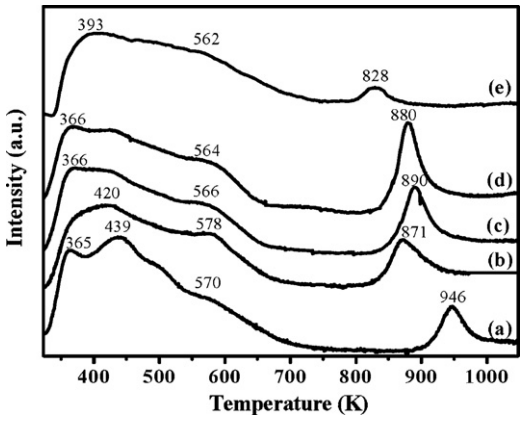

Fig. 8. NH_3-TPD profiles of: (a) Au–Cu/TiO_2 (1–1 wt.%); (b) Au–Cu/TiO_2–Fe_2O_3 (1–1 wt.%, Ti/Fe = 9/1); (c) Au–Cu/TiO_2–Fe_2O_3 (1–1 wt.%, Ti/Fe = 8/2); (d) Au–Cu/TiO_2–Fe_2O_3 (1–1 wt.%, Ti/Fe = 7/3); (e) TiO_2–Fe_2O_3 bare support (Ti/Fe = 9/1) (uncalcined, dried at 373 K; pH 7).

Table 3
Results of NH_3-TPD measurement of Au–Cu/TiO_2–Fe_2O_3 catalysts.

Catalyst	NH_3 desorbed at intermediate and low temperature region (μmol/g)	NH_3 desorbed at high temperature region (μmol/g)	Total NH_3 desorbed (μmol/g)
Au–Cu/TiO_2 (Ti/Fe = 10/0)	26.66	2.25	28.91
Au–Cu/TiO_2–Fe_2O_3(Ti/Fe = 9/1)	25.52	3.16	28.68
Au–Cu/TiO_2–Fe_2O_3(Ti/Fe = 8/2)	22.50	4.13	26.63
Au–Cu/TiO_2–Fe_2O_3(Ti/Fe = 7/3)	20.68	4.77	25.45
TiO_2–Fe_2O_3 bare support (Ti/Fe = 9/1)	26.38	0.87	27.25

tion temperature shifts to 890 and 880 K for Ti/Fe = 8/2 sample and Ti/Fe = 7/3 sample, respectively. This shows that the specific ratio of the Fe increased the strength of strong acidic sites. In the crystalline phase of $ZnMnO_3$, the presence of and Mn^{4+} and Zn^{2+}cations with a different charge/radii ratio leads to the formation of acidic sites of varying strengths [44]. We can explain the similar results by comparing the surface acidity of Au–Cu/TiO_2–Fe_2O_3 catalysts with different Ti/Fe ratios. The valence electrons for Ti^{4+} and Fe^{3+} are different and the net negative charge must be stabilized by a nearby proton or cation. The TiO_2–Fe_2O_3 mixed oxide typically terminates at the surface in the form of hydroxyl groups and structures in which oxygen is linked between Ti and Fe. The several types of Brönsted acidic sites and Lewis acidic sites can form because the variety of configurations can exist [45].

3.7. Catalytic activity

The catalytic activities of Au–Cu/TiO_2–Fe_2O_3 and Au–Cu/TiO_2 catalysts were compared for partial oxidation of methanol (POM) to produce H_2. The activities of Au–Cu/TiO_2–Fe_2O_3 catalysts with different Ti/Fe ratio, pH during preparation of the catalysts, calcination temperature and reaction temperature were also investigated. The product analysis shows that H_2 and CO_2 were the major products. H_2O and CO were formed as by-products. In addition, negligible amount of CH_4 and $HCOOCH_3$ were also detected. The CH_3OH conversion, O_2 conversion, H_2 selectivity and CO selectivity were defined below:

$$CH_3OH\ \text{conversion}\,(\%) = \left(\frac{\text{moles of } CH_3OH \text{ consumed}}{\text{moles of } CH_3OH \text{ fed}}\right) \times 100\%$$

$$O_2\ \text{conversion}\,(\%) = \left(\frac{\text{moles of } O_2 \text{ consumed}}{\text{moles of } O_2 \text{ fed}}\right) \times 100\%$$

$$H_2\ \text{selectivity}\,(\%) = \left(\frac{\text{moles of } H_2 \text{ produced} \times 0.5}{\text{moles of } CH_3OH \text{ consumed}}\right) \times 100\%$$

$$\text{CO selectivity}\,(\%) = \left(\frac{\text{moles of CO produced}}{\text{moles of } CH_3OH \text{ consumed}}\right) \times 100\%$$

The catalytic activity and product distribution in the partial oxidation of methanol (POM) over Au–Cu/TiO_2–Fe_2O_3 catalysts with different Ti/Fe ratio in the binary support were compared at 523 K. Fig. 9 shows the CH_3OH conversion and H_2 selectivity during POM over Au–Cu/TiO_2–Fe_2O_3 catalysts with different Ti/Fe ratios. It can be seen that by the addition of specific amount of Fe (Ti/Fe = 9/1), the methanol conversion was increased. However, at higher Fe content in the catalyst, the CH_3OH conversion was decreased. There is no obvious difference in H_2 selectivity with the increasing Fe amount. In general the activity of supported gold catalysts has been explained in terms of particle size Au, oxidation state of Au and metal-support interaction. Since the average particle size of Au–Cu did not altered much by the addition of Fe, the other factors should be taken into account. The increased activity by the addition of small amount of Fe could be explained in terms of higher dispersion of gold and copper thereby enhance the interaction between gold, copper and TiO_2, which increased the availability of surface oxygen [19]. The TPR results in Fig. 4 showed that the presence of Fe_2O_3 in the bimetallic system increased the reduction temperature of Au–Cu particles in the catalyst. This suggests that presence of Fe has increased the interaction between Au and Cu species. The interaction of Au with Cu eased the activation of sites due to change of redox and electronic properties of gold species [46]. This enhanced interaction increased the existence of more oxidized Au and Cu species in the catalyst as evidenced by the increased intensity of the reduction peak of oxides of Au and Cu species (Fig. 4b–d). In addition, the ease of oxygen availability was increased by the addition of small amount of Fe as evidenced by the lower reduction temperature for Fe_2O_3 to Fe_3O_4 and Fe_3O_4 to FeO compared to the reduction of bulk Fe_2O_3 in the work of Chang et al. [15]. This favorable condition was provided by a specific interaction between Au–Cu and Fe species. However, at higher addition of Fe species, the interaction of Fe species with Au and Cu species was minimized as evidenced by reduction of Fe species at higher temperature (Fig. 4c). Therefore, addition of small amount of Fe species has increased the catalytic activity of Au–Cu/TiO_2 catalyst. Several evidences were available in the literature for the increased activity of supported Au catalysts by the addition of metal oxide additives. For instance, Gluhoi et al. [47] found that Au catalysts containing reducible transition metal oxides such as CeO_x, CoO_x, MnO_x and FeO_x showed better activity, which was attributed to the ability of the transition metal oxides to provide reactive oxygen and was explained in terms of Mars and van Krevelen mechanism. In this, for most oxidation catalysts can be interpreted within the framework of this mechanism and reactive oxygen can be replaced by O_2 from the feed stream [45,48]. The influence of acidity at POM reaction can be illustrated by Table 3. The Au–Cu/TiO_2–Fe_2O_3 catalyst with the Ti/Fe = 9/1 sample is showed higher intermediate and weak acidic sites than the Ti/Fe = 8/2 and 7/3 catalyst samples. It is also showed more total acidic sites in this sample for the Au–Cu/TiO_2–Fe_2O_3 catalysts. That means the higher amount of weaker (intermediate

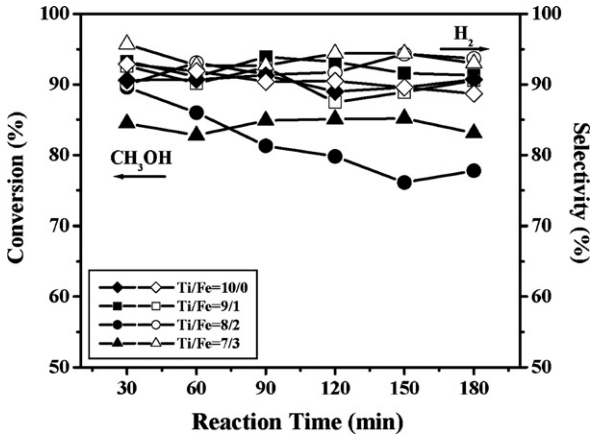

Fig. 9. Effect of Ti/Fe atomic ratio on CH_3OH conversion and H_2 selectivity for POM over Au–Cu/TiO_2–Fe_2O_3 (1–1 wt.%) catalysts (uncalcined, dried at 373 K; pH 7; O_2/CH_3OH ratio, 0.3; reaction temperature, 523 K).

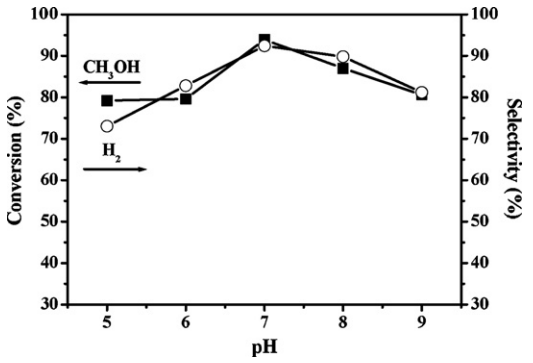

Fig. 10. Effect of pH on CH_3OH conversion and H_2 selectivity for POM over Au–Cu/TiO_2–Fe_2O_3 (1–1 wt.%, Ti/Fe = 9/1) catalysts (uncalcined, dried at 373 K; O_2/CH_3OH ratio, 0.3; reaction temperature, 523 K; reaction time, 90 min).

and weak) acidic sites and total acidic sites works as the synergistic effect to increase the CH_3OH conversion in POM reaction over Au–Cu/TiO_2–Fe_2O_3 catalysts (Ti/Fe = 9/1). The decreased methanol conversion at higher amount of Fe is also due to increase in the particle size of metal particles. Since Au–Cu/TiO_2–Fe_2O_3 catalysts with Ti/Fe = 9/1 showed higher activity, this catalyst has been used for further study.

Fig. 10 shows the catalytic activity of Au–Cu/TiO_2–Fe_2O_3 catalyst prepared at different pH values. It reveals that methanol conversion increased with increase in pH and attained maximum at pH 7, and then it decreased with further increase in pH. The H_2 selectivity was also increased with increase in pH and it dropped at pH 7. The behavior of the catalysts prepared at various pH values in methanol conversion and H_2 selectivity were explained in terms of amount of Au and Cu deposited on TiO_2–Fe_2O_3 binary support and the mean particle size at various pH values. The pH during preparation showed significant influence on the particle size and metal loading (Table 1). The lower activities at pH 5 and 6 have been explained in terms of presence of large sized metal particles on the support. Even though the catalysts prepared at high pH values (pH 8 and 9) possess small metal particles, the slightly lower activity of these catalysts might be due to lower deposition of Au on the surface of the support. Analogous effects of pH on Au particle size, gold uptake and catalytic activity was reported in the literature [49]. Since the Au–Cu/TiO_2–Fe_2O_3 catalysts prepared at pH 7 exhibited higher CH_3OH conversion and H_2 selectivity, this catalyst has been used for further study.

Fig. 11 shows the effect of calcination temperature on the catalytic activity of Au–Cu/TiO_2–Fe_2O_3 catalysts. Methanol conversion was decreased when the sample was calcined at 473 K. But there was no further change in the conversion observed at higher calcination temperatures. On the other hand, the hydrogen selectivity was decreased smoothly with increase in calcination temperature. There was an obvious increase in CO selectivity when the sample calcined at 573 K and above. These complex behaviors of the catalysts were explained by analyzing structure and morphology of the catalysts calcined at different temperatures obtained from TEM, TPR and XPS analyses. TEM analysis revealed that there is a small increase in the size of the Au–Cu particles beyond 473 K. Nevertheless, presence of copper preserves the Au–Cu particle size during calcination process to a large extent. XPS analysis illustrates that the catalyst is composed of Au^0, Au^{3+} and $Au^{\delta+}$ species with varying amount at different calcination temperatures. In uncalcined sample major portion of Au is in $Au^{\delta+}$ species. After calcinations, Au^{3+} species was completely eliminated in the sample. In addition, with increasing calcination temperature, a fraction of $Au^{\delta+}$ was converted to metallic Au. In our previous work on Au/TiO_2–Fe_2O_3 catalyst, we have identified the active species for POM in supported Au catalyst was $Au^{\delta+}$ [20]. Pestryakov and Lunin [50] also reported that in supported gold catalysts, $Au^{\delta+}$ is the active site for alcohol partial oxidation reaction. The present study also confirmed that the active species in supported gold catalyst is $Au^{\delta+}$ species. The catalyst calcined beyond 573 K showed increased CO selectivity and decreased H_2 selectivity. This is due to the combination of two factors, such as increased particle size and decreased amount of $Au^{\delta+}$ species (Tables 1 and 2). TPR analysis also evidenced the increase in particle size of Au–Cu and decrease in the amount of oxidized Au and Cu species with calcination temperatures (Fig. 5). Since the Au–Cu/TiO_2–Fe_2O_3 catalyst sample without calcination itself exhibited better performance in CH_3OH conversion and H_2 selectivity, this catalyst has been used to study the effect of reaction temperature on the catalytic activity of the catalyst.

Fig. 12 shows the CH_3OH conversion, O_2 conversion, H_2 selectivity and CO selectivity for POM over Au–Cu/TiO_2–Fe_2O_3 catalysts at temperatures between 448 and 573 K. Throughout the temperature studied O_2 consumption was virtually 100%. With increase in reaction temperature, CH_3OH conversion, H_2 selectivity and CO selectivity are increased. Methanol conversion increased from 81.8% to 96.4% and H_2 selectivity increased from 78.2% to 92.3% when the temperature increased from 448 to 573 K. There is a slow and smooth increase in CO selectivity with reaction temperature is observed. The CO selectivity is increased from 1.9% to 9.3%, when the temperature increases from 448 to 573 K. In addition, negligible amount of methane was also observed. The increase in H_2 selectivity is in three stages, which explains H_2 formation occurred by different reaction pathways. At 448 and 473 K, the H_2 selectivity is around 80% with 20% H_2O selectivity was observed. This means that

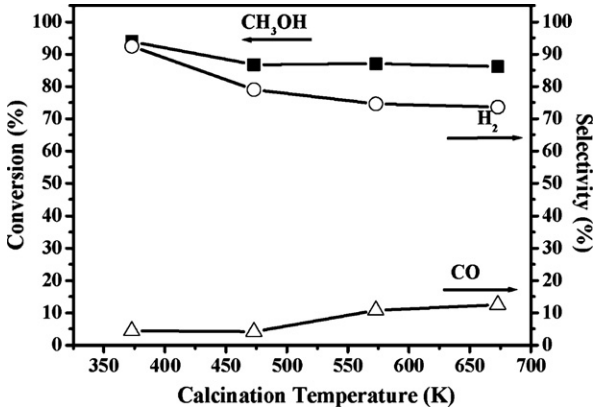

Fig. 11. Effect of calcination temperature on CH_3OH conversion, H_2 selectivity and CO selectivity for POM over Au–Cu/TiO_2–Fe_2O_3 (1–1 wt.%, Ti/Fe = 9/1) catalysts (pH 7; O_2/CH_3OH ratio, 0.3; reaction temperature, 523 K; reaction time, 90 min).

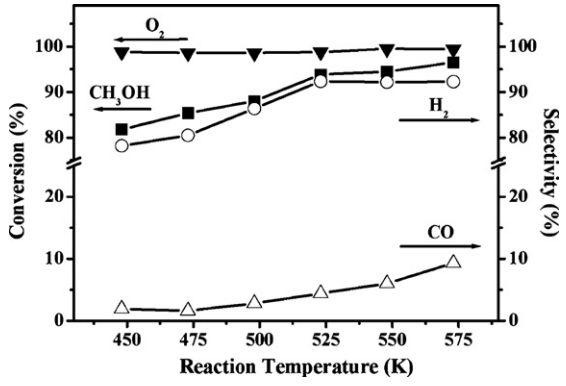

Fig. 12. Effect of reaction temperature on CH_3OH conversion, O_2 conversion, H_2 selectivity and CO selectivity for POM over Au–Cu/TiO_2–Fe_2O_3 (1–1 wt.%, Ti/Fe = 9/1) catalysts (uncalcined, dried at 373 K; pH 7; O_2/CH_3OH ratio, 0.3; reaction time, 90 min).

the highly exothermic methanol combustion (MC) (Eq. (1)) reaction had occurred parallel with POM (Eq. (2)). There is a sudden increase in H_2 selectivity was observed at 498 K with a value of 86.4%. There is further increase in H_2 selectivity when the reaction temperature increased from 498 to 523 K. The high H_2 selectivity at temperatures between 498 and 548 K implies that the steam reforming of methanol (SRM) (Eq. (3)) has involved in the reaction system. In this case, H_2O formed during MC was utilized for SRM.

$$CH_3OH + 1.5O_2 \rightarrow 2H_2O + CO_2 \quad (1)$$

$$CH_3OH + 0.5O_2 \rightarrow 2H_2 + CO_2 \quad (2)$$

$$CH_3OH + H_2O \rightarrow 3H_2 + CO_2 \quad (3)$$

At 573 K, there is a considerable increase in CO selectivity was observed. This tendency is due to the methanol decomposition (MD) (Eq. (4)) and reverse water gas shift (RWGS) (Eq. (5)) were taken place.

$$CH_3OH \rightarrow CO + 2H_2 \quad (4)$$

$$CO_2 + H_2 \leftrightarrow CO + H_2O \quad (5)$$

The Au–Cu/TiO_2–Fe_2O_3 catalysts show higher activity (82–85% CH_3OH conversion; 78–80% H_2 selectivity) at low reaction temperature region (448–473 K) compared to the Au/TiO_2–Fe_2O_3 catalysts (75–80% CH_3OH conversion; 45–59% H_2 selectivity) in our previous study [20]. It demonstrated that the Au–Cu/TiO_2–Fe_2O_3 catalysts initiate the POM reaction at lower temperature. The significant importance of this present study demonstrates that Au–Cu/TiO_2–Fe_2O_3 catalyst can be effectively applied in hydrogen production for fuel cell application at low temperature compared to previous study on POM over various supported Au, Cu and Pd catalysts [5–7,14–16,51].

4. Conclusions

The present study demonstrates that the Au–Cu/TiO_2–Fe_2O_3 catalysts are highly active compared to Au–Cu/TiO_2 catalysts. The higher activity of the Fe containing catalyst was attributed to the ability to supply reactive oxygen, thereby stabilize active gold species ($Au^{\delta+}$) in the catalyst. The optimization of Au–Cu/TiO_2–Fe_2O_3 catalysts preparation condition such as pH during preparation of the catalyst shows that the catalyst prepared at pH 7 showed high activity as this catalyst possess small metal particles and high Au loadings. The calcination process changes the chemical state and particle size of Au–Cu. There was a considerable decrease in CH_3OH conversion, H_2 selectivity and increase in CO selectivity with increasing calcination temperature. This result reveals that the uncalcined sample is active catalyst for selective formation of H_2 as it possesses more active Au species ($Au^{\delta+}$) in the catalysts. The catalytic activity at various reaction temperatures in the range of 448–573 K showed that both methanol conversion and hydrogen selectivity are increased with increasing the temperature. An apparent increase in CO selectivity was observed beyond 523 K. These results reveal that during POM other reaction mechanisms, such as methanol combustion, steam reforming of methanol and reverse water gas shift were occurred.

Acknowledgements

The authors express thanks to the Ministry of Economical Affairs of Taiwan for its financial support under contract number 95-EC-17-A-09-S1-022.

References

[1] J.C. Amphlett, K.A. Creber, J.M. Davis, R.F. Mann, B.A. Peppley, D.M. Stokes, Int. J. Hydrogen Energy 19 (1994) 131–137.
[2] J.O'M. Bockris, Int. J. Hydrogen Energy 24 (1999) 1–15.
[3] T. Shishido, Y. Yamamoto, H. Morioka, K. Takehira, J. Mol. Catal. A 268 (2007) 185–194.
[4] X. Zhang, P. Shi, J. Mol. Catal. A 194 (2003) 99–105.
[5] M.L. Cubeiro, J.L.G. Fierro, Appl. Catal. A 168 (1998) 307–322.
[6] M.L. Cubeiro, J.L.G. Fierro, J. Catal. 179 (1998) 150–162.
[7] J. Agrell, K. Hasselbo, K. Jansson, S.G. Jaras, M. Boutonnet, Appl. Catal. A 211 (2001) 239–250.
[8] Z. Wang, J. Xi, W. Wang, G. Lu, J. Mol. Catal. A 191 (2003) 123–134.
[9] T. Tsoncheva, V. Mavrodinova, L. Ivanova, M. Dimitrov, S. Stavrev, C. Minchev, J. Mol. Catal. A 259 (2006) 223–230.
[10] T. Tsoncheva, S. Areva, M. Dimitrov, D. Paneva, I. Mitov, M. Linden, C. Minchev, J. Mol. Catal. A 246 (2006) 118–127.
[11] T.L. Reitz, S. Ahmed, M. Krumpelt, R. Kumar, H.H. Kung, J. Mol. Catal. A 20 (2000) 275–285.
[12] L. Alejo, R. Lago, M.A. Peña, J.L.G. Fierro, Appl. Catal. A 162 (1997) 281–297.
[13] R. Ubago-Pérez, F. Carrasco-Marín, C. Moreno-Castilla, Catal. Today 123 (2007) 158–163.
[14] S.D. Lin, A.C. Gluhoi, B.E. Nieuwenhuys, Catal. Today 90 (2004) 3–14.
[15] F.-W. Chang, L.S. Roselin, T.-C. Ou, Appl. Catal. A 334 (2008) 147–155.
[16] T.-C. Ou, F.-W. Chang, L.S. Roselin, J. Mol. Catal. A 293 (2008) 8–16.
[17] A. Venugopal, J. Aluha, M.S. Scurrel, Catal. Lett. 90 (2003) 1–6.
[18] P. Haider, A. Baiker, J. Catal. 248 (2007) 175–187.
[19] M.M. Schubert, S. Hackenberg, A.C. van Veen, M. Muhler, V. Plzak, R.J. Behm, J. Catal. 197 (2001) 113–122.
[20] F.-W. Chang, H.-Y. Yu, L.S. Roselin, H.-C. Yang, T.-C. Ou, Appl. Catal. A 302 (2006) 157–167.
[21] V.R. Choudhary, V.P. Patil, P. Jana, B.S. Uphade, Appl. Catal. A 350 (2008) 186–190.
[22] X. Liu, O. Korotkikh, R. Farrauto, Appl. Catal. A 226 (2002) 293–303.
[23] E.V. Golubina, E.S. Lokteva, V.V. Lunin, N.S. Telegina, A.Yu. Stakheev, P. Tundo, Appl. Catal. A 302 (2006) 32–41.
[24] F.-W. Chang, H.-Y. Yu, L.S. Roselin, H.-C. Yang, Appl. Catal. A 290 (2005) 138–147.
[25] M. Kosmulski, J. Colloid Interface Sci 275 (2004) 214–224.
[26] S. Ivanova, V. Pitchon, C. Petit, J. Mol. Catal. A 256 (2006) 278–283.
[27] C.K. Chang, Y.J. Chen, C.T. Yeh, Appl. Catal. A 174 (1998) 13–23.
[28] C. Baatz, U. Brüße, J. Catal. 249 (2007) 34–40.
[29] F. Moreau, G.C. Bond, Catal. Today 122 (2007) 260–265.
[30] J. Llorca, M. Domínguez, C. Ledesma, R.J. Chimentão, F. Medina, J. Sueiras, I. Angurell, M. Seco, O. Rossell, J. Catal. 258 (2008) 187–198.
[31] L.H. Chang, N. Sasirekha, Y.W. Chen, Catal. Commun. 8 (2007) 1702–1710.
[32] G.J. Hutchings, M.S. Hall, A.F. Carley, P. Landon, B.E. Solsona, C.J. Kiely, A. Herzing, M. Makkee, J.A. Moulijn, A. Overweg, J.C. Fierro-Gonzalez, J. Guzman, B.C. Gates, J. Catal. 242 (2006) 71–81.
[33] A. Wolf, F. Schüth, Appl. Catal. A 226 (2002) 1–13.
[34] J. Hua, K. Wei, Q. Zheng, Z. Lin, Appl. Catal. A 259 (2004) 121–130.
[35] G.P. Xu, Y.X. Zhu, J. Ma, H.G. Yan, Y.C. Xie, Stud. Surf. Sci. Catal. 112 (1997) 333–338.
[36] J. Xiaoyuan, L. Guanglie, Z. Renxian, M. Jianxin, C. Yu, Z. Xiaming, Appl. Surf. Sci. 173 (2001) 208–220.
[37] J.F. Moulder, W.F. Stickle, P.E. Sobol, K.D. Bomben, J. Chastain, R.C. King Jr., Handbook of X-ray Photoelectron Spectroscopy, Physical Electronics, Inc., Eden Prairie, MN, 1992.
[38] A.M. Visco, F. Neri, G. Neri, A. Donato, C. Milone, S. Galvagno, Phys. Chem. Chem. Phys. 1 (1999) 2869–2873.
[39] Z. Mekhalif, F. Sinapi, F. Laffineur, J. Delhalle, J. Electron Spectrosc. Relat. Phenom. 121 (2001) 149–161.
[40] R.G. Herman, K. Klier, G.W. Simmons, P.B. Finn, J.B. Bulko, T.P. Kobylinski, J. Catal. 56 (1979) 407–429.
[41] F. Raimondi, K. Geissler, J. Wambach, A. Wokaun, Appl. Surf. Sci. 189 (2002) 59–71.
[42] P. Berteau, B. Delmon, Catal. Today 5 (1989) 121–137.
[43] L.S. Cheng, R.T. Yang, N. Chen, J. Catal. 164 (1996) 70–81.
[44] M.A. Peña, J.L.G. Fierro, Chem. Rev. 101 (2001) 1981–2017.
[45] C.N. Satterfield, Heterogeneous Catalysis in Industrial Practice, second ed., McGraw-Hill, New York, 1991.
[46] E. Smolentseva, N. Bogdanchikova, A. Simakov, A. Pestryakov, I. Tusovskaya, M. Avalos, M.H. Farías, J.A. Díaz, V. Gurin, Surf. Sci. 600 (2006) 4256–4259.
[47] A.C. Gluhoi, N. Bogdanchikova, B.E. Nieuwenhuys, J. Catal. 229 (2005) 154–162.
[48] G.C. Bond, D.T. Thompson, Gold Bull. 2 (2000) 41–51.
[49] C. Cellier, S. Lambert, E.M. Gaigneaux, C. Poleunis, V. Ruaux, P. Eloy, C. Lahousse, P. Bertrand, J.-P. Pirard, P. Grange, Appl. Catal. B 70 (2007) 406–416.
[50] A.N. Pestryakov, V.V. Lunin, J. Mol. Catal. A 158 (2000) 325–329.
[51] H.-C. Yang, F.-W. Chang, L.S. Roselin, J. Mol. Catal. A 276 (2007) 184–190.